THE JOURNAL OF PHYSICAL CHEMISTRY A

ARTICLE

pubs.acs.org/JPCA

Dipolar Solute Rotation in a Supercritical Polar Fluid

Amit Das, Ranjit Biswas,* and J. Chakrabarti

Department of Chemical, Biological and Macromolecular Sciences, S. N. Bose National Centre for Basic Sciences, Block JD, Sector III, Salt Lake, Kolkata-700 098, India

Supporting Information

ABSTRACT: Fluorescence anisotropy measurements reveal a nonmonotonic density dependence for average rotation time (τ_R) of a polar solute, coumarin153 (C153) in polar supercritical fluoroform (CHF_3). The conventional Stokes−Einstein−Debye model, relating τ_R to the solvent viscosity, fails to explain the observed density dependence, because the experimental viscosity increases monotonously with density for a fluid, in general. Here, the density-dependent τ_R is calculated by incorporating the wave vector-dependent viscosity of the solvent and the solute−solvent interaction. A molecular hydrodynamic description is used for the wave vector-dependent viscosity which is verified by molecular dynamics (MD) simulation. A justification for the applicability of the present prescription is provided by reproducing the experimental viscosity of supercritical (SC) CHF_3. Solute−solvent interaction has been included via the fluctuating torque acting on the rotating solute. Incorporation of wave vector-dependent viscosity leads to a qualitative description of the experimental density dependence of τ_R which is further improved upon inclusion of solute−solvent interaction.

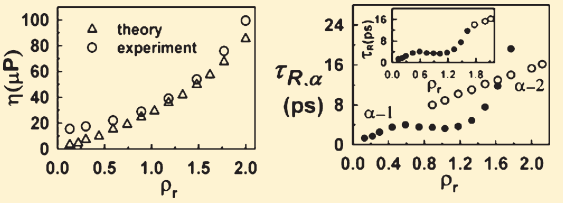

1. INTRODUCTION

A fluid phase slightly above the gas−liquid critical temperature is broadly regarded as a SC fluid.[1] It is highly compressible, offering large tunability of density by mild pressure variations. Pedagogically, the solvent−density dependence of several nonequilibrium rate processes near room temperature can be studied in SC fluids like carbon dioxide, fluoroform, ethane, etc., having a critical temperature (T_c) close to room temperature.[2] Specifically, rotational dynamics of aromatic solutes in a SC fluid can supply valuable information regarding the nature of solute−solvent coupling[3−5] and the local environment of the solute. For fluorescent solutes in different media, the rotational dynamics of the solute is usually followed by measuring the time-dependent fluorescence anisotropy[6] $r(t)$. In the case of large solutes, $r(t)$ generally follows an exponential decay, with a characteristic time scale for the solute rotation. Sometimes there can be multiexponential decay. One then obtains via time integration of the normalized $r(t)$ an average rotational correlation time, τ_R, conventionally called the rotation time. This τ_R is dominated by the longer time scale in the case of a multiexponential decay.

The $r(t)$ decay of C153 (Coumarin 153) in SC CHF_3 has been reported[7] to be single exponential for all solvent densities. The observed τ_R is nearly temperature insensitive with a nonmonotonic variation between 5 and 9 ps as the fluid density (ρ) increases. In spite of large uncertainties, there is a clear maximum near ρ_r (=ρ/ρ_c, ρ_c being the critical density of the fluid) = 0.6 with $\tau_R \approx 8$ ps and a minimum around $\rho_r = 1.0$ with $\tau_R \approx 5$ ps. The conventional Stokes−Einstein−Debye (SED) model[4,7−10] for solute rotation predicts for a spherical rotor in the limit of stick boundary condition[10] $\tau_R = \eta V_p/k_BT$, where η is the shear viscosity of the solvent, V_p the molecular volume of the rotor, and k_BT the Boltzmann constant times the absolute temperature. Since η for a fluid including the SC fluids in general monotonically increases[11] with density, this model fails to explain the above complex density dependence of τ_R in SC CHF_3 (T_c = 299 K).[2]

The SED model has two major drawbacks:

(1) Being based on a purely continuum description of the molecular solvent, it does not consider the effects of solvent structure on τ_R. The SC fluids have large compressibility. In a fluid composed of spherical molecules of diameter σ, the spatial arrangement of molecules can be described by the wave vector (k) dependent static structure factor,[12−14] $S(k\sigma)$. Note that the compressibility is the long-wavelength limit of $S(k\sigma)$. Therefore, $S(k\sigma)$ may have a crucial role in the observed complex density dependence of τ_R.

(2) The solute−solvent interaction has not been included in the above model. Several workers attempted[3−5,15−18] to incorporate the effects of solute−solvent interaction on solute rotation. In particular, the concept of dielectric friction[19] has been invoked to address the change in the friction experienced by a rotating polar solute due to electrostatic interactions. However, none of the above works conclusively support this picture. Relatively recent work[17] suggests that the additional friction due to solute−solvent interaction is attributable to a static 'electrostriction' effect. This is believed to originate from the enhanced solvent structure in the first solvation shell[20]

Received: September 10, 2010
Revised: December 24, 2010
Published: January 21, 2011

Scheme 1. Pictorial Description of Solute−Solvent Interaction Effects on Solute Rotation[a]

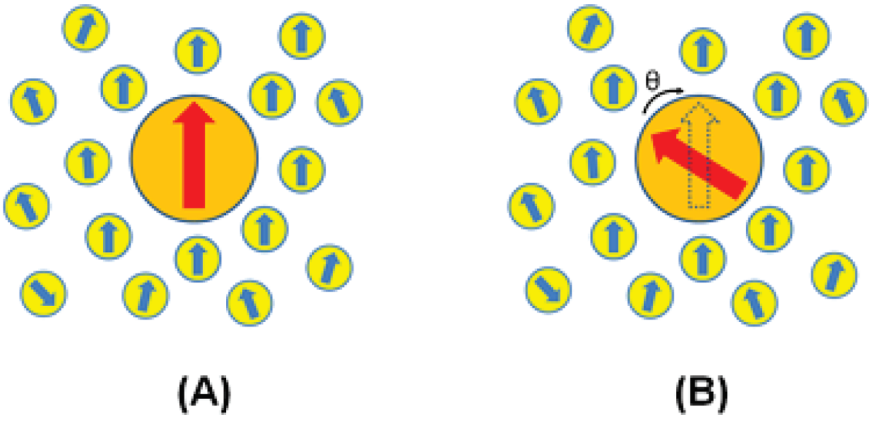

[a] Smaller circles with smaller arrows denote the solvent dipoles, whereas larger circles with larger arrows denote the solute dipole. (A) The equilibrium condition with solute in its excited state. (B) After an angular displacement (θ) of the solute dipole in the background of solvent molecules.

around the solute due to electrical interaction between the solute and the solvent molecules. Another interesting factor encouraging inclusion of solute−solvent interaction is the 'local density augmentation' (LDA)[2,4,7,9,21−27] observed during solvation in a SC solvent. As one approaches the critical density from low ρ_r, the solvent density around a dissolved solute becomes much larger than the bulk density of the SC solvent. This unusual enhancement of local density is termed as the LDA. For C153 in SC CHF_3, the maximum in τ_R and LDA occurs[2] around the same ρ_r. Note that such LDA is an outcome of strong solute−solvent coupling overcoming large length scale density fluctuations near the critical point. Therefore, the solute−solvent interaction may have a significant role in solute rotation in a SC polar fluid. Note that a modified SED model[4,10] includes the effects of solute−solvent interaction via two phenomenological parameters: a boundary condition factor and a solute shape factor.

Here, we introduce a theoretical framework to calculate the τ_R of a polar solute in a polar fluid incorporating the contributions of both solvent structure and solute−solvent dipolar interaction. Basically, the same conventional SED theory is used with a couple of ramifications.

(1) The hydrodynamic viscosity η is replaced with the wave vector-dependent viscosity $\eta(k\sigma)$ of the fluid which brings in $S(k\sigma)$ directly into the picture. This is done based on molecular hydrodynamic arguments, leading to an analytical expression of $\eta(k\sigma)$ which is verified via a MD simulation. We also show how to extract the experimental η for a SC fluid from $\eta(k\sigma)$. This modification to the SED model captures qualitatively the experimentally observed nontrivial density dependence of τ_R in SC CHF_3.

(2) The effect of the solute−solvent interaction is included by considering the rotational relaxation of the excited solute in fluorescence depolarization experiments. In such experiments, anisotropy in polarization is created by photoexciting a dissolved solute. This anisotropy in polarization subsequently relaxes to a new equilibrium via rotational diffusion of the solute. Let us consider a small angular displacement of the solute dipole from its final solvent-equilibrated orientation in the background of the solvent dipoles (see Scheme 1). The solute dipole would then tend to relax back to its equilibrium orientation by rotational diffusion under the action of torque generated via the solute−solvent interaction.

2. WAVE VECTOR-DEPENDENT VISCOSITY

a. Case of a Normal Liquid. Let us first consider $\eta(k\sigma)$ of a normal liquid. According to molecular hydrodynamics, the transverse current autocorrelation function $C_\perp(k\sigma,t)$ is defined as $C_\perp(k\sigma,t) = k^2\langle j_\perp^k(t) j_\perp^{-k}(0)\rangle$, where $j_\perp^k(t)$ is the Fourier component of the transverse current. Now, $C_\perp(k\sigma,t)$ is known to be related to the shear viscosity η of the fluid[12]

$$C_\perp(k\sigma,t) = \omega_0^2 e^{-\nu k^2 t} \quad (1)$$

where t denotes the time, $\omega_0^2 = k^2(k_B T/m)$, $\nu = \eta/\rho m$, and m is the mass of a fluid molecule. Integrating both sides of eq 1 over the entire time range we get the wave vector-dependent viscosity given by[28]

$$\eta(k\sigma) = \frac{\rho m}{k^2}\left[\frac{1}{\omega_0^2}\int_0^\infty C_\perp(k\sigma,t)\mathrm{d}t\right]^{-1} \quad (2)$$

Fick's law[12] for diffusive motion states that the current

$$\vec{j}(\vec{r},t) = -D\vec{\nabla}\rho(\vec{r},t) \quad (3)$$

where $\rho(\vec{r},t)$ is the time-dependent microscopic solvent density at position $\vec{r}$, D being the self-diffusion coefficient of the fluid. Now, eq 3 yields in the Fourier space for the transverse current, $j_\perp^k(t) = ik_\perp D\rho_k(t)$, $k_\perp$ being the transverse component of $\vec{k}$ (parallel to z axis). Multiplying both sides by $j_\perp^{-k}(0)$ and taking the average over the initial conditions, we obtain

$$\langle j_\perp^k(t) j_\perp^{-k}(0)\rangle = k_\perp^2 D^2\langle\rho_k(t)\rho_{-k}(0)\rangle \quad (4)$$

It is known[12] that $\rho_k(t) = \rho_k e^{-Dk^2 t}$, ρ_k being the Fourier component of the microscopic solvent density. Inserting this in eq 4 leads to $\langle j_\perp^k(t) j_\perp^{-k}(0)\rangle = k_\perp^2 D^2 S(k\sigma) e^{-Dk^2 t}$, where static structure factor $S(k\sigma) = \langle\rho_k\rho_{-k}\rangle$.[12] Thus, we reach at a molecular hydrodynamic expression of $C_\perp(k\sigma,t)$, following its definition[12]

$$C_\perp(k\sigma,t) = k^2\langle j_\perp^k(t) j_\perp^{-k}(0)\rangle = k^2 k_\perp^2 D^2 S(k\sigma) e^{-Dk^2 t} \quad (5)$$

Putting eq 5 in eq 2 and performing the integration one obtains

$$\eta(k\sigma) = \frac{\rho k_B T}{k_\perp^2 D S(k\sigma)} \quad (6)$$

dx.doi.org/10.1021/jp1086398 |J. Phys. Chem. A 2011, 115, 973–978

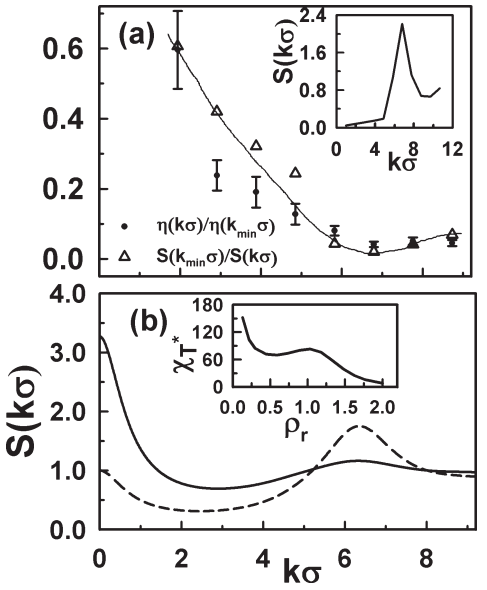

Figure 1. (a) $\eta(k\sigma)/\eta(k_{min}\sigma)$ (filled circles with error bars) and $S(k_{min}\sigma)/S(k\sigma)$ (open triangles, the solid line is drawn only as a guide to the eyes) as a function of $k\sigma$, both calculated from MD simulation, for LJ liquid for $\rho\sigma^3 = 0.8$ at 96 K. (Inset) $S(k\sigma)$ of the same system calculated from our simulation. (b) $S(k\sigma)$ as a function of $k\sigma$ for SC CHF_3 at 310 K at two densities: $\rho_r = 0.74$ (solid line) and 2.0 (the dotted line). (Inset) Scaled compressibility χ_T^* of SC CHF_3 at 310 K as a function of ρ_r.

We set $k_\perp^2 = 6\pi\rho r_0$ (ρ being the bulk density and r_0 the molecular radius of the fluid) to arrive at the final expression of wave vector-dependent viscosity

$$\eta(k\sigma) = \frac{k_B T}{6\pi D r_0 S(k\sigma)} \tag{7}$$

We can also derive the weakly interacting limit of diffusion reported in ref 14 from the expression of $\eta(k\sigma)$: The isothermal compressibility of the fluid[12] is given by $\chi_T = \lim_{k\sigma\to 0}(\rho k_B T)^{-1} S(k\sigma)$. Thus, $\eta(k\sigma \approx 0) = k_B T/6\pi r_0 D S(k\sigma \approx 0) = 1/(6\pi r_0 D\rho\chi_T)$. Rearranging this we get $D = \Gamma_d/\rho^2\chi_T$, where $\Gamma_d = \rho/6\pi r_0\eta$, a density-dependent dissipative coefficient introduced in ref 14.

Note that eq 7 yields

$$\eta(k\sigma)/\eta(k'\sigma) = S(k'\sigma)/S(k\sigma) \tag{8}$$

for wave vectors $k\sigma$ and $k'\sigma$. In the long-wavelength $k\sigma \approx 0$ limit where $S(k\sigma)$ has a minimum[12] (inset, Figure 1a), an expansion yields $\eta(k\sigma) \propto (1 - bk^2\sigma^2)$, where b depends on the curvature of $S(k\sigma)$ near $k\sigma \approx 0$. Such small $k\sigma$ behavior of $\eta(k\sigma)$ has been reported earlier.[28,29]

Both sides of eq 8 can be computed from molecular dynamics simulations which can provide a direct test of the wave vector-dependent viscosity. We consider to this end, for simplicity, a Lennard−Jones (LJ) system at normal liquid condition. The interaction potential between a pair of LJ liquid molecules at separation r is given by $4\varepsilon[(\sigma/r)^{12} - (\sigma/r)^6]$, ε being the interaction strength parameter.[12] Our simulation system involves 216 LJ particles using the argon units[12] [ε = 120K in k_B unit, diameter σ = 3.4 Å, and molecular mass 40 amu], adopting NVE ensemble.[12] A simple cubic simulation box is used of side $L = 6.46\sigma$ with the periodic boundary condition on all sides. The density of the system is taken at $\rho\sigma^3 = 0.8$ and the average temperature at $k_B T/\varepsilon \approx 0.8$ (96 K). The equations of motion are integrated using the Verlet algorithm,[30] the time step for integration being 0.0215 ps.

We calculate $\eta(k\sigma)$ from the simulation by eq 2 where $C_\perp(k\sigma,t) = k^2\langle j_\perp^k(t) j_\perp^{-k}(0)\rangle$. The Fourier component of the current is given by $j_\perp^k(t) = \sum_i v_i^\perp(t) e^{-ikz_i(t)}$, $v_i^\perp(t)$ being the transverse component of the velocity of the ith particle at time t and $z_i(t)$, its z coordinate at time t. Finally, we can write $C_\perp(k\sigma,t) = k^2\langle\sum_i v_i^\perp(0) e^{-ikz_i(0)}\sum_j v_j^\perp(t) e^{ikz_j(t)}\rangle$. Here, the angular brackets represent an average over 1000 independent initial configurations. The structure factor $S(k\sigma)$ has been calculated from the Fourier transform (FT) of the pair correlation function[12,30] obtained via the simulations.

The finiteness of the simulated system size restricts us to explore the $k\sigma \approx 0$ limit.[28] The minimum accessible wave vector in our simulation is $k_{min}\sigma = 2\pi\sigma/L$, L being the side length of the simple cubic simulation box. The inset in Figure 1a shows $S(k\sigma)$ from the simulations. Figure 1a shows a comparison between $\eta(k\sigma)/\eta(k_{min}\sigma)$ (circles with error bars) and $S(k_{min}\sigma)/S(k\sigma)$ (open triangles), both computed from the simulations. Both plots are similar in appearance with almost the same rate of decrease from the maximum value of unity at the smallest wave vector, which is consistent with the low wave vector expansion. The discrepancy between the two plots is more pronounced for the low wave vector region, which could be due to finite size effects in the simulations.[30]

b. Extension to SC CHF_3. As hydrodynamic results are insensitive to the detailed molecular interactions, we expect the hydrodynamic description of $\eta(k\sigma)$ to be valid for SC polar fluids also. To this end we locate the critical point[31] of the polar fluid from the divergence of χ_T at the critical condition. We calculate $S(k\sigma)$ using the standard liquid-state theory[12] and obtain its $k\sigma \approx 0$ limit as a theoretical estimate of χ_T. Here, $S(k\sigma)$ is computed using the Ornstein−Zernike[12,13] relation: $S(k\sigma) = [1 - \rho C(k\sigma)]^{-1}$, $C(k\sigma)$ being the Fourier transform (FT) of $C(r)$, the spatial direct correlation function of the fluid. In our calculation we assume that the solvent−solvent interaction consists of a hard-core part of diameter σ and a longer ranged dipolar contribution due to a dipole moment of magnitude μ located at the center of a solvent molecule. $C(r)$ is expressed as a combination of the short-ranged and longer-ranged part for the polar fluid. For the former, we use the Percus−Yevick (PY)[12,13] form $C^{PY}(r)$ for hard-sphere potential, while the latter $C^{LR}(r)$ is derived from the angle-averaged Mayer's function[12,13] based on the standard dipolar potential

$$C(r) = C^{PY}(r) + C^{LR}(r) \tag{9}$$

where

$$C^{PY}(r) = c_0 + c_1(r/\sigma) + c_3(r/\sigma)^3 \quad \text{for } r < \sigma \tag{10}$$
$$= 0 \quad \text{for } r > \sigma$$

and

$$C^{LR}(r) = 2\mu^4/9(k_B T)^2 r^6 \tag{11}$$

The three coefficients c_0, c_1, and c_3 in $C^{PY}(r)$ are functions of the packing fraction $p = (\pi/6)\rho\sigma^3$ and given by $c_0 = -(1 + 2p)^2/(1-p)^4$, $c_1 = 6p(1 + 0.5p)^2/(1-p)^4$, and $c_3 = 0.5pc_0$. The inset of Figure 1b shows $\chi_T^*(=\chi_T\mu^2/\sigma^6)$ for a typical isotherm. Our estimate for the critical point is $T_c^*(=k_B T_c\sigma^3/\mu^2) = 0.29$ and $\rho_c^* = 0.25$, which are in good agreement with the experimental numbers.[11] The details of all these calculations are given in section I of the Supporting Information.

dx.doi.org/10.1021/jp1086398 |J. Phys. Chem. A 2011, 115, 973–978

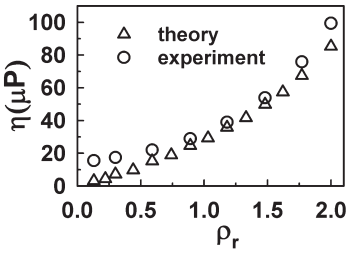

Figure 2. Experimentally measured[11] shear viscosity (circles) and theoretically calculated shear viscosity (triangles) of SC CHF_3 (σ = 3.5 Å),[11] both at 310 K, as a function of ρ_r.

Subsequently, we perform calculations at a supercritical temperature.[31] We show the calculated $S(k\sigma)$ of SC CHF_3 in Figure 1b at two densities above and below ρ_c. In general, two peaks can be observed in $S(k\sigma)$: one around $k\sigma \approx 0$ in a region dominated by fluid compressibility and another around $k\sigma \approx 2\pi$ dictated by the molecular packing. For low ρ_r, the peak at $k\sigma \approx 0$ predominates which gradually disappears with increasing ρ_r along with the concomitant enhancement of the packing-driven peak.

We use this $S(k\sigma)$ and experimentally observed[11] D to obtain $\eta(k\sigma)$ for SC CHF_3. It is found that the experimentally observed shear viscosity of SC CHF_3 is well reproduced (see Figure 2) by an integration of $\eta(k\sigma)$ over the entire range of wave vectors: $\bar{\eta} = (1/4\pi)\int \eta(k\sigma)d\vec{k}\sigma / \int d\vec{k}\sigma$, where the factor $1/4\pi$ takes care of the degeneracy of the choice of the transverse direction. Here, for numerical purposes, the integration range was taken from $k\sigma = 0$ to $k\sigma = 10$. We note that a larger upper limit does not alter the value of $\bar{\eta}$. The experimentally observed viscosity is thus an average momentum transfer in a given layer of fluid over all length scales. This rationalizes the extension of the molecular hydrodynamic expression for $\eta(k\sigma)$ for SC CHF_3.

c. Rotation Time Scales in SC CHF_3. Let us now consider the generalization of the SED theory via replacement of η by $\eta(k\sigma)$. Recalling the SED expression of $\tau_R = \eta V_p/k_BT$, we can define the rate of rotational relaxation $\omega = 1/\tau_R = k_BT/\eta V_p$. Introducing $\eta(k\sigma)$ we get the wave vector-dependent rate $\omega(k\sigma) = k_BT/\eta(k\sigma)V_p$. Now, the different peaks in $S(k\sigma)$ for SC CHF_3, both sharp and broad, appearing at different regions of wave vectors, create different wave vector windows for $\omega(k\sigma)$. We average the $\omega(k\sigma)$ over the wave vectors under a given structure factor peak to produce an average rate $\tilde{\omega}_{av,\alpha} = \int_\alpha \omega(k\sigma)d\vec{k}\sigma / \int_\alpha d\vec{k}\,\sigma$ for the αth peak. The rotation time for the αth peak is then $\tilde{\tau}_{R,\alpha} = 1/\tilde{\omega}_{av,\alpha}$. Here, each of the structure factor peaks (see Figure 1b) will give rise to a time scale implying an overall multiexponential rotational relaxation. For example, at the low-density region ($\rho_r < 1$), $S(k\sigma)$ has a single prominent peak around $k\sigma \approx 0$ but no such peak at larger wave vectors. This implies a single-exponential relaxation, τ_R being governed by the single peak. In the higher density region ($\rho_r > 1$), the relaxation would be biexponential with two time scales because of two peaks in $S(k\sigma)$, τ_R being a weighted average of the two. However, the present formalism does not allow calculating the weights of these separate time scales.

Figure 3a shows both $\tilde{\tau}_{R,1}$ and $\tilde{\tau}_{R,2}$ of C153 in SC CHF_3 at 310 K as a function of ρ_r, while the experimental data at two temperatures 302 and 310 K are shown in the inset. At very low densities, $k\sigma \approx 0$ being the only peak of $S(k\sigma)$, $\tilde{\tau}_{R,1}$ is the only relevant time scale. Interestingly, it shows all the features of the

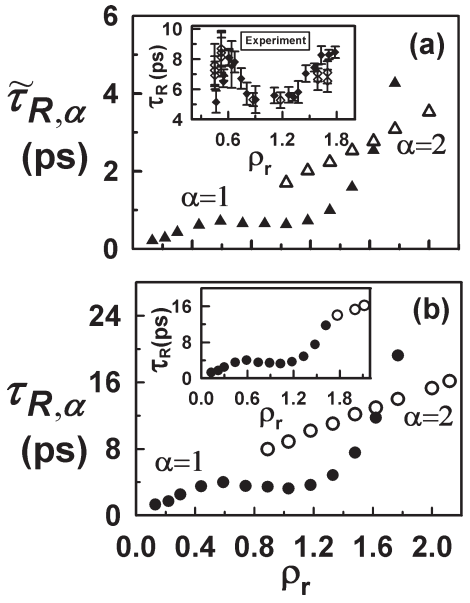

Figure 3. (a) Rotation times of C153 (V_p = 246 Å^3)[32] in SC CHF_3 calculated from the SED model with η being replaced by $\eta(k\sigma)$ at 310 K as a function of ρ_r: Filled and open triangles represent the $\tilde{\tau}_{R,1}$ (from $k\sigma \approx 0$ peak) and $\tilde{\tau}_{R,2}$ ($k\sigma \approx 2\pi$ peak), respectively. (Inset) Experimentally observed time scales (filled and open diamonds with error bars at 302 and 310 K). (b) Rotation times of C153 (μ_0 = 13.4D)[24] in SC CHF_3 calculated after inclusion of solute−solvent polar interaction at 310 K: Filled and open circles represent $\tau_{R,1}$ and $\tau_{R,2}$, respectively. (Inset) Lower time scale of $\tau_{R,1}$ and $\tau_{R,2}$, the symbols being identical as before.

experimental density dependence of rotation time with the maximum at ρ_r = 0.59, agreeing qualitatively with the experimental data. The appearance of this maximum can be explained by a minimum in compressibility (see inset of Figure 1b). Such a minimum also justifies the LDA becoming maximum near ρ_r = 0.6. $\tilde{\tau}_{R,1}$ becomes a minimum at ρ_r = 1.03, with good agreement with the experimental finding. This minimum is explained by the maximum in compressibility at ρ_r = 1.03.

The packing-dominated peak appears for densities above ρ_r = 1, giving rise to $\tilde{\tau}_{R,2}$ that increases linearly with ρ_r. In this regime the packing-dominated contribution of $S(k\sigma)$ remains almost unchanged with density implying $\tilde{\tau}_{R,2} \propto 1/D$. According to Enskog's description,[12] $D = [3/(8\rho\sigma^2 g(\sigma))](k_BT/\pi m)^{1/2}$ for a fluid where $g(\sigma)$ is the radial distribution function at contact, m being the mass of a molecule. As $g(\sigma)$ is weakly sensitive to ρ_r in this density regime, we get $\tilde{\tau}_{R,2} \propto 1/D \propto \rho_r$. Note that in the density range $0 < \rho_r < 1.6$, $\tilde{\tau}_{R,1}$ and $\tilde{\tau}_{R,2}$ do not differ significantly from each other, although $\tilde{\tau}_{R,1} < \tilde{\tau}_{R,2}$. However, $\tilde{\tau}_{R,1}$ increases rapidly at very high densities ($\rho_r > 1.6$) where the fluid becomes highly incompressible. The experimental τ_R in these densities does not show such rapid increase but rather is comparable in trend with $\tilde{\tau}_{R,2}$.

3. SOLUTE−SOLVENT INTERACTION

Next we include the solute−solvent interaction. The torque on the solute dipole undergoing rotational relaxation, as shown in Scheme 1, is determined by the interaction energy, $U(\theta)$, of the rotating photoexcited dipolar solute (with excited state dipole moment μ_0) as a function of its orientation θ (with respect to the laboratory frame z axis) due to the solvent dipoles (dipole

moment μ) in the first solvation shell (see section II, Supporting Information). $U(\theta)$ depends on two factors:

(1) the solute−solvent dipolar interaction potential[33] and
(2) the solvent orientation distribution in the first solvation shell.

The solvent orientation is characterized by $\rho_{10}(t)$, the projection of the solvent orientation distribution for spherical harmonic $l = 1$. Since we are considering the perturbation from the final equilibrium orientation of the solute and relaxation back to the same equilibrium state, we use overdamped equation of motion for all the relevant dynamical variables. Note that the solvent orientation distribution undergoes relaxation as well, the rate being dictated by the solvent rotational diffusion D_R. The fluctuating torque is then given by $-\partial U(\theta)/\partial\theta$, where $U(\theta) = -u_0\rho_{10}(t)\rho_0 \cos\theta$ (see section II, Supporting Information), where $\rho_0 = 1/4\pi$, the bulk value of the orientation profile. The overdamped equation of motion of the solute dipole: $\Gamma_{rot}\dot{\theta} = -\partial U(\theta)/\partial\theta$, where Γ_{rot} is the rotational frictional coefficient.[34,35] For small angular displacement (θ) from the final equilibrium state and $t < D_R^{-1}$, the solution is $\theta(t) = \theta(0)e^{-\omega t}$. Here $\omega = u_0\rho_0\rho_{10}(0)/\Gamma_{rot}$, the angular frequency of rotation which is the relaxation rate of the orientational correlation function. Hence, we identify $\tau_R = 1/\omega = \eta V_p M/k_B T$, where[36] $M = \pi(6k_BTR^3/\mu_0\mu)^2(1-2\ \mu^2\rho/9k_BT)$, R being the solute−solvent interaction length in the first solvation shell (see section II, Supporting Information). This expression is similar to the SED expression, with the friction experienced by the solute dipole being modified by a factor of M over the hydrodynamic friction. Therefore, the solute−solvent interaction contributes nonadditively to the hydrodynamic friction.[17] Now, inserting the $k\sigma$ dependence we get the modified wave vector-dependent rotational relaxation frequency: $\omega(k\sigma) = k_BT/\eta(k\sigma)V_pM$ and follow the similar averaging over peaks of $S(k\sigma)$ to calculate the new time scales $\tau_{R,1}$ and $\tau_{R,2}$. To calculate M we use $R = R_0 + r_0$, R_0 and r_0 being the solute and solvent radii, respectively. Figure 3b shows the $\tau_{R,1}$ and $\tau_{R,2}$. The maximum in $\tau_{R,1}$ is now at 4 ps at $\rho_r = 0.59$, and the minimum is at 3.24 ps at $\rho_r = 1.03$. The $\tau_{R,2}$ values ranges between 9 and 16 ps for $\rho_r \geq 1.6$. Interestingly, the experimental τ_R of C153 compares well to the lower of the two calculated time scales. In particular, the large time scale given by $\tau_{R,1}$ has not been reported in the experiments for $\rho_r \geq 1.6$. Thus, identification of τ_R with $\tau_{R,1}$ for low density and that with $\tau_{R,2}$ at high density produces semiquantitative agreement with the experimental data, shown in the inset of Figure 3b.

4. CONCLUSION

We developed a theoretical understanding of the rotational relaxation for large polar solutes in polar SC solvents incorporating the solvent structure via wave vector-dependent shear viscosity and then the solute−solvent interaction. Here we extend the SED picture to incorporate the molecular interactions explicitly. The SED model, in its conventional form, can qualitatively produce the experimental data with the simple replacement of η by $\eta(k\sigma)$. However, for a semiquantitative agreement one needs to include the solute−solvent interaction. Apart from extracting the time scales that compare well with the experimental data, the present theory explains the possible causes behind this remarkable density dependence of rotation of a polar solute in a SC polar fluid. In particular, the rotational relaxation of the solute at low solvent densities is essentially governed by fluid compressibility. We predict that at very high densities where the packing dominates the solvent structure, the time scales increase linearly. We expect that a more explicit treatment of the solute−solvent interaction would yield a better agreement to the experimental rotation times.[3] Even though we restrict our discussion to rotation of C153 in SC fluoroform for the availability of experimental data, the present theoretical framework is applicable to rotation of a polar solute in a polar solvent in general. Moreover, such framework can be used to find the rotation time in other systems having different solute−solvent interactions and different solvent structures, like electrolytes and ionic liquids to name only a few.

■ ASSOCIATED CONTENT

Supporting Information. Details of necessary derivations. This material is available free of charge via the Internet at http://pubs.acs.org.

■ AUTHOR INFORMATION

Corresponding Author

*Phone: 91 33 2335 5706. Fax: 91 33 2335 3477. E-mail: ranjit@bose.res.in; rbsnbc@gmail.com.

■ ACKNOWLEDGMENT

A.D. thanks the Council of Scientific and Industrial Research, India, for a research fellowship. R.B. thanks M. Maroncelli for several useful suggestions.

■ REFERENCES

(1) Noyori, R., Ed. *Chem. Rev.* **1999**, *99*, 353-354.
(2) Biswas, R.; Lewis, J. E.; Maroncelli, M. *Chem. Phys. Lett.* **1999**, *310*, 485–494.
(3) Kurnikova, M. G.; Balabai, N.; Waldeck, D. H.; Coalson, R. D. *J. Am. Chem. Soc.* **1998**, *120*, 6121–6130.
(4) Horng, M. L.; Gardecki, J. A.; Maroncelli, M. *J. Phys. Chem. A* **1997**, *101*, 1030–1047.
(5) Maroncelli, M. *J. Chem. Phys.* **1997**, *106*, 1545–1555.
(6) Lakowicz, J. R. *Principles of Fluorescence Spectroscopy*; Kluwar Academic/Plenum Publishers, New York, 1999.
(7) Kometani, N.; Hoshihara, Y.; Yonezawa, Y.; Kajimoto, O.; Hara, K.; Ito, N. *J. Phys. Chem. A* **2004**, *108*, 9479–9483.
(8) Debye, P. *Polar Molecules*; Chemical Catalog Co.: New York, 1929.
(9) deGrazia, J. L.; Randolph, T. W.; O'Brien, J. A. *J. Phys. Chem. A* **1998**, *102*, 1674–1681.
(10) Dote, J. L.; Kivelson, D.; Schwartz, R. N. *J. Phys. Chem.* **1981**, *85*.
(11) Song, W.; Patel, N.; Maroncelli, M. *J. Phys. Chem. B* **2002**, *106*, 8783–8789.
(12) Hansen, J. P.; McDonald, I. R. *Theory of Simple Liquids*, 3rd ed.; Academic: San Diego, 2006.
(13) Gray, C. G.; Gubbins, K. E. *Theory of Molecular Fluids*; Oxford University Press: New York, 1984.
(14) Chaikin, P. M.; Lubensky, T. C. *Principles of Condensed Matter Physics*; Cambridge University Press: Cambridge, 1995.
(15) Papazyan, A.; Maroncelli, M. *J. Chem. Phys.* **1995**, *102*, 2888–2919.
(16) Balabai, N.; Sukharevsky, A.; Read, I.; Strazisar, B.; Kurnikova, M.; Hartman, R. S.; Coalson, R. D.; Waldeck, D. H. *J. Mol. Liq.* **1998**, *77*, 37–60.
(17) Kumar, P. V.; Maroncelli, M. *J. Chem. Phys.* **2000**, *112*, 5370–5381.
(18) Kurnikova, M. G.; Waldeck, D. H.; Coalson, R. D. *J. Chem. Phys.* **1996**, *105*, 628–638.

(19) Nee, T. W.; Zwanzig, R. *J. Chem. Phys.* **1970**, *52*, 6353–6363.
(20) Marcus, Y. *Chem. Rev.* **1988**, *88*, 1475–1498.
(21) Betts, T. A.; Zagrobelny, J.; Bright, F. V. *J. Am. Chem. Soc.* **1992**, *114*, 8163–8171.
(22) Heitz, M. P.; Bright, F. V. *J. Phys. Chem.* **1996**, *100*, 6889–6897.
(23) Heitz, M. P.; Maroncelli, M. *J. Phys. Chem. A* **1997**, *101*, 5852–5868.
(24) Ingrosso, F.; Ladanyi, B. M.; Mennucci, B.; Scalmani, G. *J. Phys. Chem. B* **2006**, *110*, 4953–4962.
(25) Kometani, N.; Arzhantsev, S.; Maroncelli, M. *J. Phys. Chem. A* **2006**, *110*, 3405–3413.
(26) Lewis, J. E.; Biswas, R.; Robinson, A. G.; Maroncelli, M. *J. Phys. Chem. B* **2001**, *105*, 3306–3318.
(27) Patel, N.; Biswas, R.; Maroncelli, M. *J. Phys. Chem. B* **2002**, *106*, 7096–7114.
(28) Gaskell, T.; Balucani, U.; Gori, M.; Vallauri, R. *Phys. Scr.* **1987**, *35*, 37–39.
(29) Halle, B.; Davidovic, M. *Proc. Natl. Acad. Sc. U.S.A.* **2003**, *100*, 12135–12140.
(30) Allen, M. P.; Tildsley, D. J. *Computer Simulation of Liquids*; Clarendon Press: Oxford, 1887.
(31) Biswas, R.; Chakrabarti, J. *J. Phys. Chem. B* **2007**, *111*, 13743–13747.
(32) Horng, M. L.; Gardecki, J. A.; Papazyan, A.; Maroncelli, M. *J. Phys. Chem.* **1995**, *99*, 17311–17337.
(33) Note that the total solute−solvent interaction contains an orientation-independent short-ranged component in addition to the asymmetric (dipolar) component. However, the short-ranged component does not contribute to the torque acting on the solute because the latter (torque) is determined by the angle-dependent interaction alone.
(34) Cantor, C. R.; Schimmel, P. R. *Biophysical Chemistry*; W. H. Freeman: New York, 1980; Part II.
(35) Mukherjee, A.; Bagchi, B. *Curr. Sci.* **2006**, *91*, 1208–1216.
(36) Here, an obvious restriction arises, out of the mean field approximations we imposed in our formulation, to allow only positive values of the factor M that $2\mu^2\rho/9k_BT < 1$.